

# A COMPARATIVE STUDY OF CRUCIFORM AND ANNULAR PARACHUTES: EVALUATING DRAG AND STABILITY PERFORMANCES

Ee Kui Wei<sup>1</sup>, Quah Zhi Cong Ebenezer<sup>2</sup>, Lee Jian Ming<sup>2</sup>

<sup>1</sup>Methodist Girls' School, 11 Blackmore Drive Singapore 599986

<sup>2</sup>DSO National Laboratories, 12 Science Park Drive Singapore 118225

---

## Abstract

Over the years, parachutes have evolved and various designs have been developed. One of the main applications is in cargo drops, allowing equipment to land safely. The two main types of parachutes used in this application are the cruciform and annular parachute. This study investigates and compares the drag and stability characteristics of a rigid cruciform and annular parachute under varying angles of attack. Through conducting Computational Fluid Dynamics (CFD) simulations and experimental drop tests, cruciform parachutes, with a cross-shaped canopy, displayed higher drag coefficients and stability compared to annular parachutes of the same projected area. Using the Shear Stress Transport (SST) K-omega model, CFD simulations revealed a drag coefficient of 1.87 and 1.6 for the cruciform and annular parachute respectively, which is supported by a 98.4% agreement between CFD data and experimental data.

## 1. Introduction

Parachutes are utilised in a wide range of applications, such as military and recreational activities. Playing a critical role in parachute recovery systems for Unmanned Aerial Vehicles (UAVs) and aerial deliveries, various parachute designs have been designed, investigated, and improved by researchers to enhance the performance of parachutes in different conditions [1-3]. One of the key applications is in cargo drops, where parachutes are used to ensure that the equipment stays intact. Among the different parachute designs, the prominent parachute designs used for cargo drops are annular and cruciform. The cruciform parachute, with its cross-shaped canopy, allows for a more uniform distribution of pressure across the surface, decreasing the number of oscillations during descent. Thus, displaying higher stability characteristics than the annular parachute, which has a ring-shaped canopy, in most cases. This is supported by a study conducted in 1981 where cruciform parachutes, tested in wind-tunnel conditions and behind wake-producing bodies like the A-21 cargo container, demonstrated high stability characteristics while still yielding high drag [4]. While being known for their use as decelerators, some have started investigating their potential as gliders [5-6] and using them to make precise deliveries [7].

Given the pivotal role that drag and stability characteristics of a parachute plays in cargo drop operations, this study aims to investigate and compare the drag force and stability characteristics of annular and cruciform parachutes at various angles of attack (aoa) by conducting controlled Computational Fluid Dynamics (CFD) simulations. Data is then validated through experimental test. The findings of this study will contribute to a better understanding of the aerodynamic performance of these parachute designs, providing insights that could enhance their applications in military, humanitarian, and commercial cargo drops.

## 2. Hypothesis

The cruciform parachute possesses a higher stability and drag coefficient ( $C_d$ ) than the annular parachute with the same projected area ( $A$ ).

### 3. Methodology

#### 3.1 Parachute Models

An initial estimation of the required size of the parachute was calculated using the standard equation:

$$Fd = \frac{C_d}{2} \rho v^2 A \quad (1)$$

Using a  $C_d$  value of 0.85 from existing literature [8], while assuming the descent rate of the parachute ( $v$ ) and density of air ( $\rho$ ) to be 5.0m/s and 1.225 kg/m<sup>3</sup> respectively, with the drag force ( $Fd$ ) being equal to the weight of the whole parachute system, 2.5N, the projected area is found as shown below:

$$2.5 = \frac{0.85}{2} \times 1.225 \times 5^2 A$$

$$A = 0.19207m^2 \text{ (5sf)}$$

The radius is thus calculated for the final diameter to be found using the equation:

$$A = \pi r_{big}^2 - \pi r_{voidspaces}^2$$

As the arm ratio of the cruciform parachute is 2, width of parachute ( $w$ ) = 0.5 length of parachute = the radius of the big circle ( $r_{big}$ ) = 2(radius of small circle formed by void spaces) ( $r_{voidspaces}$ )

$$0.19207 = \pi w^2 - \pi \frac{w^2}{4}$$

$$w = 0.280m \text{ (3sf)}$$

Thus, obtaining an initial parachute size, where length of parachute = 0.560 m. The model was then used to run a CFD simulation and drag force obtained was two times the drag force needed to allow the whole parachute system to descend at the speed of 5m/s. Hence, parachute area was halved, obtaining the parameters shown in Table 1. To ensure that results obtained are precise, the parachutes are scaled up by 25% as well as 50%. The reference length and area used to calculate the drag and moment coefficients are the diameter of the parachute and projected area respectively.

Table 1: Summary of parachute parameters

Parachute Design	Cruciform			Annular		
	A	B	C	A	B	C
Nominal diameter, $D_o$ (m)	0.40	0.50	0.60	0.348	0.435	0.522
Projected Area (m <sup>2</sup> )	0.094248	0.14726	0.21206	0.094164	0.147131	0.21187
Arm width, $W$ (m) = 1/2 $D_o$ (m)	0.20	0.25	0.30			

Spill hole diameter, $D_s$ (m) = 0.1 $D_o$				0.0348	0.0435	0.0522
---	--	--	--	--------	--------	--------

Note: (Conceptual design of both parachutes in Appendix)

Design A: Baseline diameter

Design B: 25% more than baseline diameter

Design C: 50% more than baseline diameter

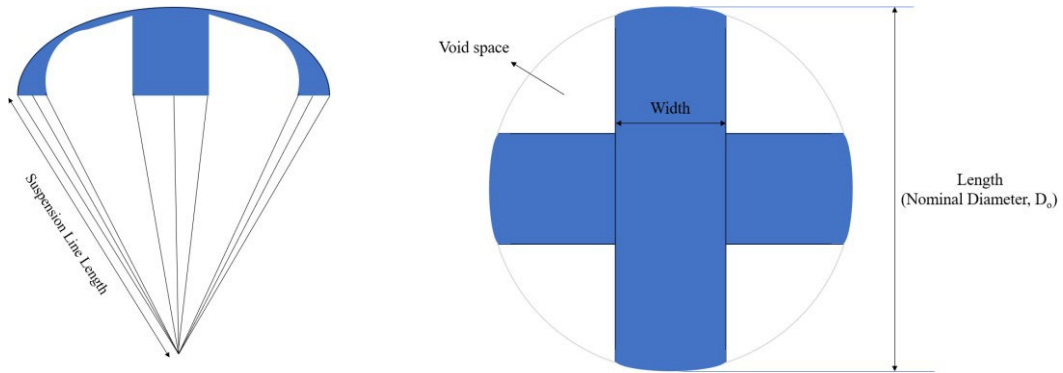


Fig. 1.1: Conceptual design of cruciform parachute when inflated

### 3.2 Mesh Generation

Mesh quality plays an important role in sustaining stability and accuracy of CFD simulations. Hence, in this study, three meshes of different grid resolution types, as can be seen in Fig. 2, Table 2.1 and 2.2 in appendix, were generated and compared. Cell size near the geometry is small, gradually increasing toward the stationary domain region. As there is an insignificant change in the forces in, and moments about, the x, y and z axes for the different meshes, the coarsest mesh, Mesh C, was used for the following CFD simulations for efficiency.

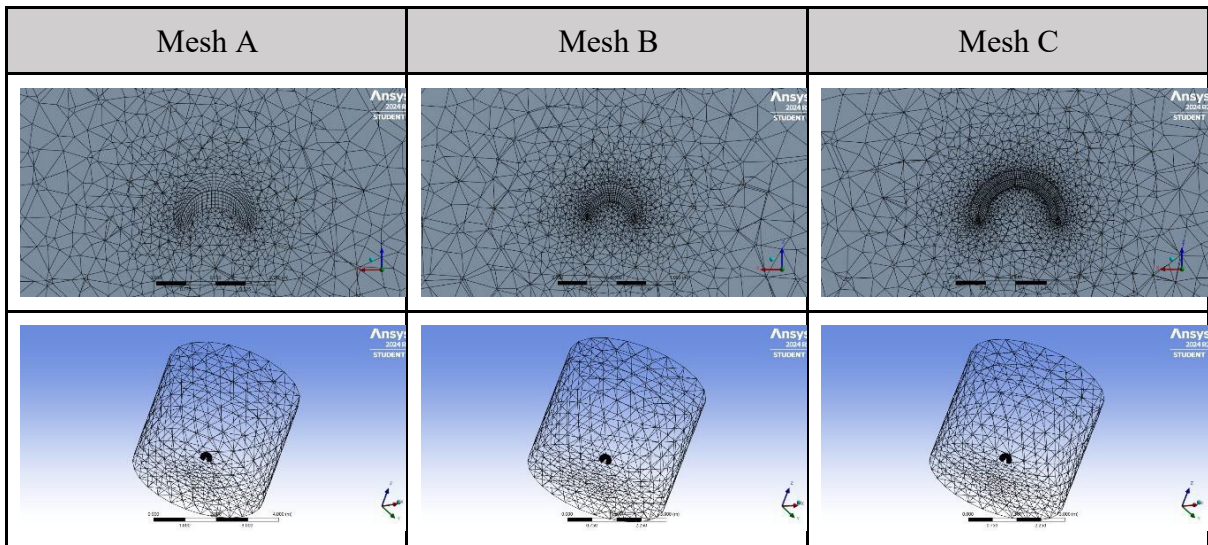


Fig. 2: Mesh refinement for cruciform parachute

Table 2.1: Values of the three forces and three moments in/about x, y, z axes at 0 aoa

Canopy design	Mesh	Nodes	Elements	$\bar{F}_z$ (N)	$\bar{F}_y$ (N)	$\bar{F}_x$ (N)	Mx	My	$\bar{M}_z$
Cruciform	Coarse (A)	10114	43083	2.69	0.00595	0.00535	-0.000119	0.000124	-0.0000409
	Medium (B)	16867	68723	2.70	0.0126	0.00211	-0.000219	0.0000634	0.00000196
	Fine (C)	70259	235196	2.68	0.0122	0.00856	-0.000000852	-0.0000756	-0.0000323

### 3.3 Computational Fluid Dynamics (CFD) Simulation

In this simulation, it is assumed that the parachute cannot deform and there was no exchange of heat with the velocity of steady incoming airflow being 5m/s and density of air being 1.225kg/m<sup>3</sup>. Simulation platform used was Ansys Students 2024R2 and the Shear Stress Transport (SST) K-omega model was used to replicate real-life conditions where there is a high probability of turbulence due to environmental factors such as the physical terrain or other man-made structures [9-10]. The SST K-omega model combines the advantages of both the k-omega and k-epsilon turbulence models, making it suitable for simulations involving boundary layer flows and adverse pressure gradients. The model has two governing equations which are the turbulent kinetic energy:

$$\frac{\partial k}{\partial t} + U_j \frac{\partial k}{\partial x_j} = P_k - \beta^* k \omega + \frac{\partial}{\partial x_j} \left[ (\nu + \sigma_k \nu_T) \frac{\partial k}{\partial x_j} \right]$$

and the specific dissipation rate as shown below:

$$\frac{\partial \omega}{\partial t} + U_j \frac{\partial \omega}{\partial x_j} = \alpha S^2 - \beta \omega^2 + \frac{\partial}{\partial x_j} \left[ (\nu + \sigma_\omega \nu_T) \frac{\partial \omega}{\partial x_j} \right] + 2(1 - F_1) \sigma_{\omega 2} \frac{1}{\omega} \frac{\partial k}{\partial x_i} \frac{\partial \omega}{\partial x_i}$$

Initial values of turbulent kinetic energy and specific dissipation rate were set to be 0.09375 and 641.8003 respectively and fluid air flows in the positive z-direction at 0 aoa. For the change in aoa, fluid air is set to flow in y and z axes. Simulation was also set to run till all lines converged as seen in Fig. 3 and 4 (refer to appendix).

### 3.4 Experimental Drop-Test

A real-life drop test was conducted using the Arduino Nano BLE contained in a 3D-printed box and data was collected using the onboard IMU in the Arduino. The 3D payload box was made using PLA material and used to store the components of the payload. A cruciform parachute was made using ripstop nylon, following the parameters of design A, with a suspension line length of 0.35m. The parachute, seen in Fig. 5 of Appendix, was dropped from a height of ~14 metres, at 0 aoa, with the weight of the whole system being 0.312 kg.

#### 4. Results and Discussion

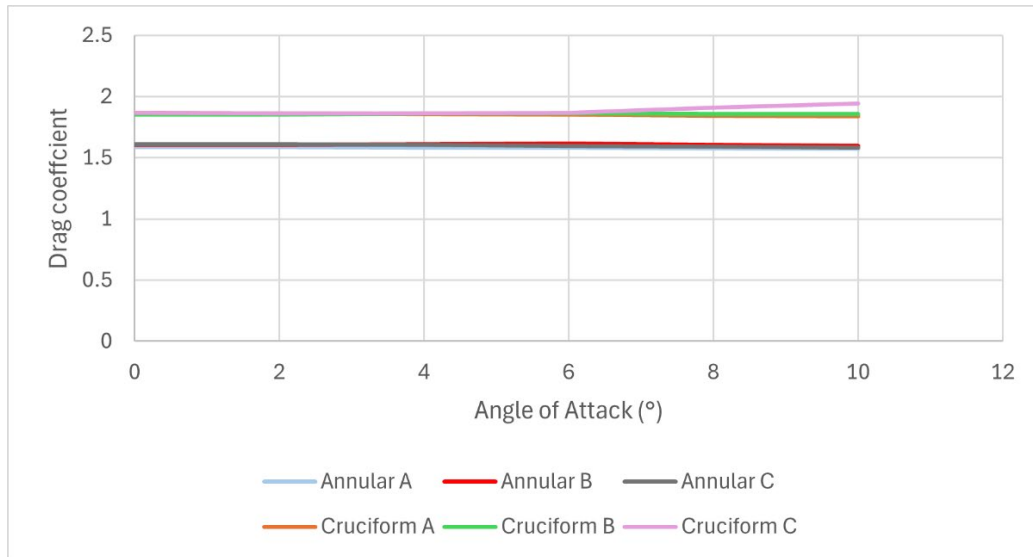


Fig. 6.1: Graph of drag coefficient against aoa from CFD

Data generated suggest that a cruciform parachute would experience a higher average drag coefficient of 1.87 as compared to an annular parachute, experiencing a lower average drag coefficient of 1.6. This may be because the cruciform parachute only has parts removed nearer to the outer edge where pressure difference between top and bottom surface is lower, compared to the annular parachute, of which the center part is removed, where difference in pressure is the highest. This means that the pressure difference on the cruciform parachute is higher than that on the annular parachute, resulting in the cruciform parachute generating a higher drag. Furthermore, the coinciding lines for the three different parachute sizes for each type of parachute indicate that the calculated drag coefficient is accurate and consistent.

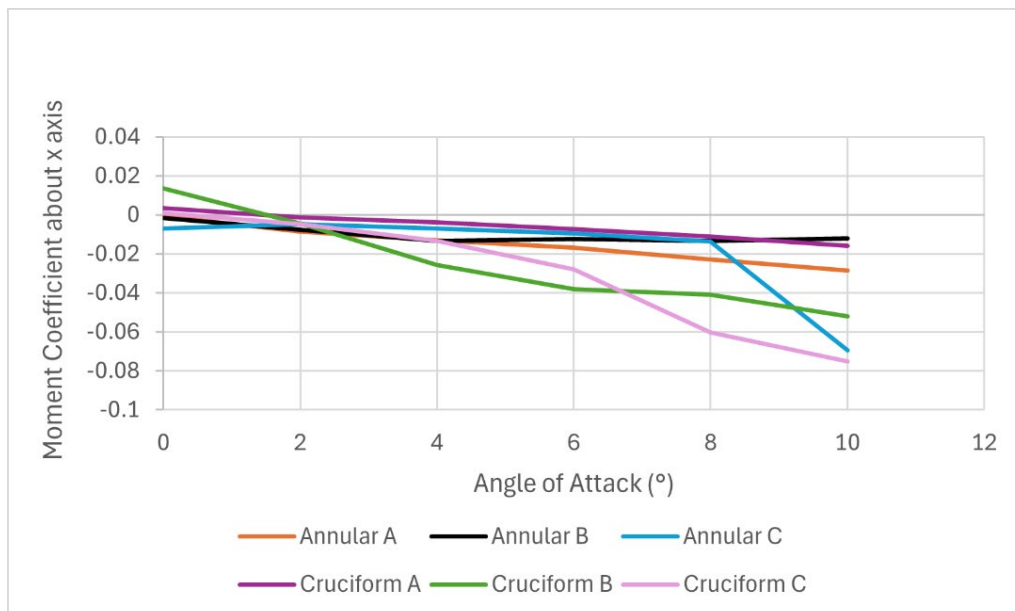
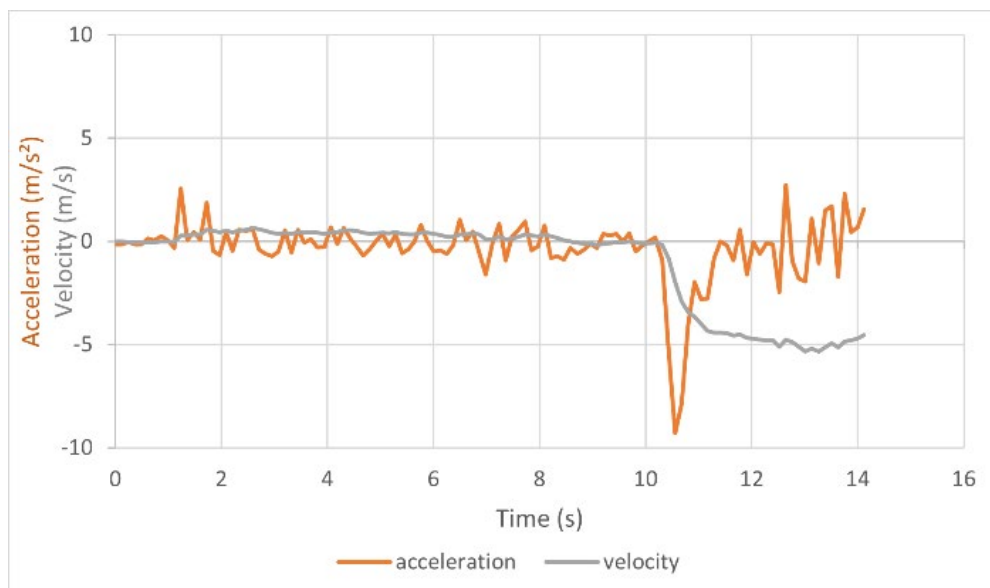


Fig. 6.2: Graph of moment coefficient about x-axis against aoa from CFD

In Fig 6.2, it is observed that cruciform parachutes B and C have a higher negative moment coefficient about the  $x$ -axis than the two corresponding annular parachutes, B and C. This

suggests that the cruciform parachute generates a higher restoring moment than the annular parachute when it encounters crosswinds. Hence, with the same projected area, it can be implied that the cruciform parachute displays a higher stability than the annular parachute. A possible explanation could be that due to the cross-shape that the arms of a cruciform parachute are arranged in, extending from the central point, a more asymmetric surface area than the annular parachute is created. Hence, when the parachute descends, the flow of air over the parachute canopy creates different pressure distributions on each arm, generating differing drag forces as angle of attack changes. This drag creates a restoring moment that counteracts unwanted oscillatory motions, allowing increasing the stability performance of the cruciform parachute. However, according to Fig. 6.2, annular A has a higher stability than cruciform A. This may be due to the fixed offset distance, which results in the centre of mass being relatively further away from the parachute when parachute size is smaller, thus allowing the annular parachute to be relatively stable.



*Fig. 6.3: Graph of acceleration and velocity in  $m/s^2$  and  $m/s$  respectively, against time in seconds from experimental data*

A drop test was conducted and the results are presented in Fig. 6.3. The parachute is dropped at  $\sim 10s$ , where acceleration increased sharply to  $-9.3m/s^2$ . An exponential curve, representing velocity, is observed to reach a terminal velocity of  $\sim 5.3m/s$  at  $13.0s$ . A drag coefficient of  $1.9$  was obtained from experimental data using equation (1), showing good agreement with data collected from CFD simulations, where the drag coefficient is  $1.87$ . The difference of only  $1.6\%$  shows close correspondence, validating the reliability of both experimental methodology and computational model. However, the plot terminates early, and ground impact could not be observed in the acceleration and velocity curve. This could be due to the shock caused by the impact resulting in a stop in the data logging process.

## **5.2 Conclusion & Further research**

In this study, two types of parachutes, cruciform and annular, were compared in terms of drag and stability performance. While significant insights were gained, several existing key limitations may have affected experimental data, such as the deformation of parachute canopy and cloth permeability [11], which was not accounted for in CFD simulations. Furthermore, due to the processing speed and load shedding process of the Arduino which resulted in some time intervals varying by 12-13ms, there are unavoidable inconsistencies in time intervals between data points, possibly affecting the data trend observed. Moreover, the true aoa of the parachute at the start of the drop is unable to be determined due to wind and oscillation of parachute and the exact orientation of the IMU is challenging to ascertain. Additionally, trajectory data obtained using an IMU tends to drift overtime, which can affect the accuracy of the data trend observed. As the current study is done with the assumption of a rigid parachute canopy, more investigation should be done on the dynamic stability to analyse the oscillatory effects of a cruciform parachute.

## References

- [1] Fields, Travis D., and Oleg A. Yakimenko. "The Use of a Steerable Single-Actuator Cruciform Parachute for Targeted Payload Return." *2017 IEEE Aerospace Conference*, Mar. 2017, <https://doi.org/10.1109/aero.2017.7943787>.
- [2] Britting, Thomas, et al. "Selection Criteria for Parachutes of Student-Built Sounding Rockets." *4th Symposium on Space Educational Activities*, 1 Apr. 2022, <https://doi.org/10.5821/conference-9788419184405.133>.
- [3] Fields, Travis D., and Oleg A. Yakimenko. "Development of a Steerable Single-Actuator Cruciform Parachute." *Journal of Aircraft*, vol. 55, no. 3, Oct. 2017, pp. 1041–1049, <https://doi.org/10.2514/1.c034416>.
- [4] Herrington, Shawn, et al. "Modeling and Control of a Steerable Cruciform Parachute System through Experimental Testing." *AIAA Scitech 2019 Forum*, 6 Jan. 2019, <https://doi.org/10.2514/6.2019-1074>.
- [5] JORGENSEN, D., & COCKRELL, D. (1981). *Aerodynamics and performance of cruciform parachute canopies*. <https://doi.org/10.2514/6.1981-1919>
- [6] Potvin, J, et al. *Glide Performance Study of Standard and Hybrid Cruciform Parachutes*. 19 May 2003, <https://doi.org/10.2514/6.2003-2160>. Accessed 17 Sept. 2023.
- [7] Haller, Joseph, et al. *Precision Aerial Delivery with a Steerable Cruciform Parachute*. 2 June 2017, <https://doi.org/10.2514/6.2017-3539>.
- [8] Saim, R, et al. "Computational Fluid Dynamic (CFD) Analysis on ALUDRA SR-10 UAV with Parachute Recovery System." *IOP Conference Series: Materials Science and Engineering*, vol. 243, Sept. 2017, p. 012014, <https://doi.org/10.1088/1757-899x/243/1/012014>.
- [9] Yu, Hesheng, and Jesse Thé. "Validation and Optimization of SST K- $\omega$  Turbulence Model for Pollutant Dispersion within a Building Array." *Atmospheric Environment*, vol. 145, Nov. 2016, pp. 225–238, <https://doi.org/10.1016/j.atmosenv.2016.09.043>.
- [10] Halim, M. A., Mohd, N., Mohd, & Md. Nizam Dahalan. (2018). *The Evaluation of k- $\epsilon$  and k- $\omega$  Turbulence Models in Modelling Flows and Performance of S-shaped Diffuser*. 15(2), 5161–5177. <https://doi.org/10.15282/ijame.15.2.2018.2.0399>
- [11] Ludtke, W. P. (1971). *Effects of Canopy Geometry on the Drag Coefficient of a Cross Parachute in the Fully Open and Reefed Conditions for a W/L Ratio of 0.264*.

## Appendix

*Table 1: Summary of parachute parameters*

Parachute Design	Cruciform			Annular		
	A	B	C	A	B	C
Nominal diameter, $D_o$ (m)	0.40	0.50	0.60	0.348	0.435	0.522
Projected Area ( $m^2$ )	0.094248	0.14726	0.21206	0.094164	0.147131	0.21187
Arm width, $W$ (m) = $1/2 D_o$ (m)	0.20	0.25	0.30			
Spill hole diameter, $D_s$ (m) = $0.1 D_o$				0.0348	0.0435	0.0522

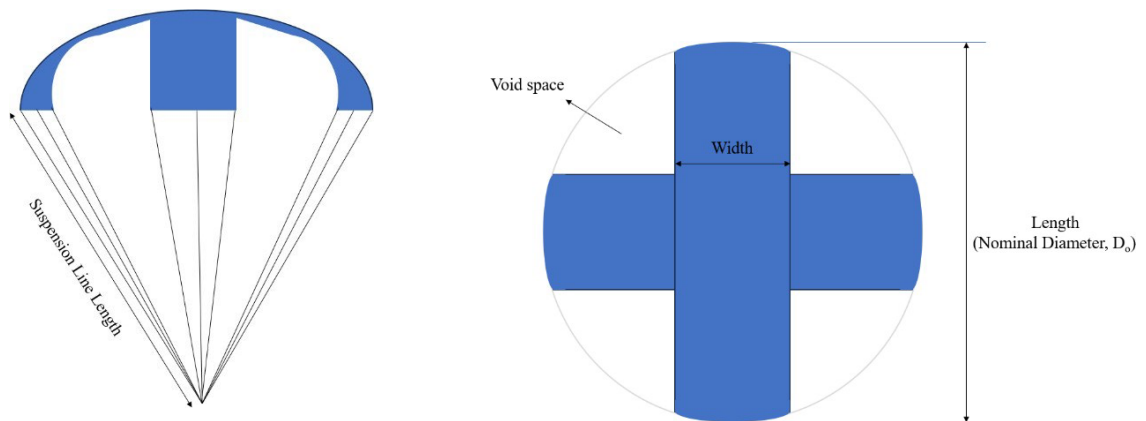


*Fig. 1.1: Conceptual design of cruciform parachute when inflated*

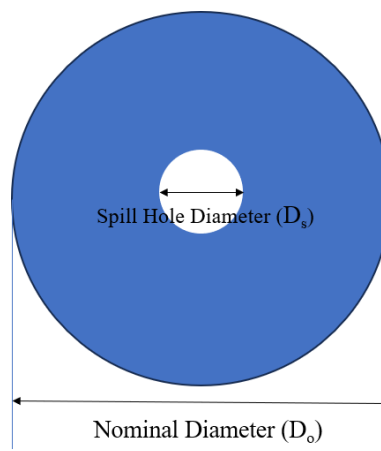


*Fig. 1.2: Conceptual design of inflated annular parachute*

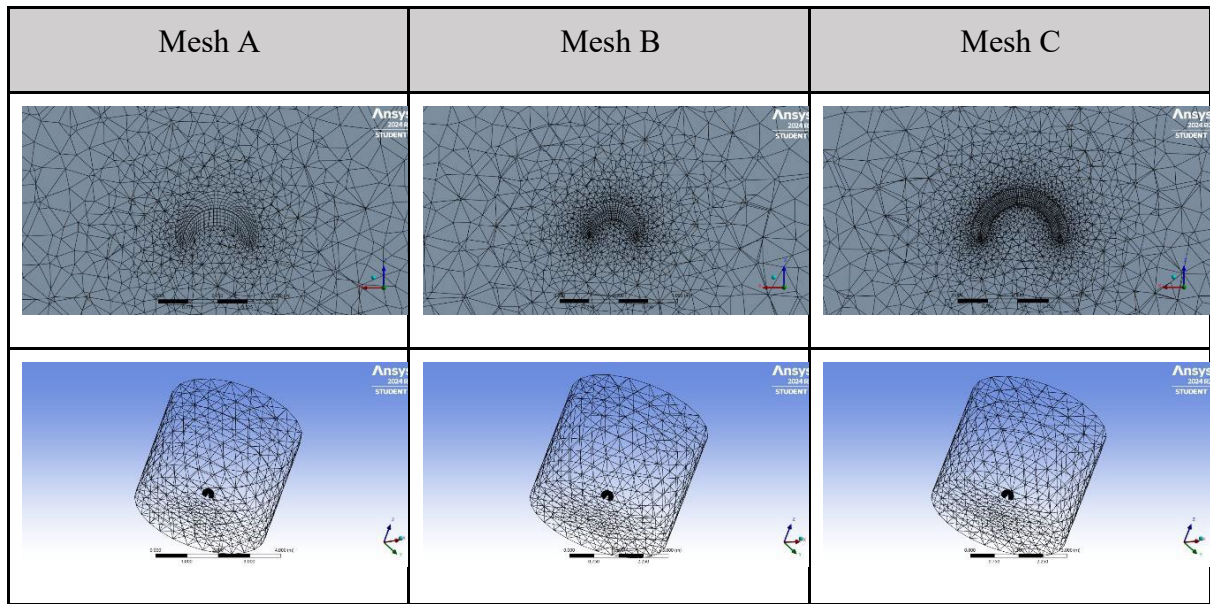


Fig. 2: Mesh refinement for cruciform parachute

Table 2.1: Values of the three forces and three moments in/about x, y, z axes at 0 aoa for cruciform parachute

Canopy design	Mesh	Nodes	Elements	$F_z$ (N)	$F_y$ (N)	$F_x$ (N)	Mx	My	Mz
Cruciform	Coarse (A)	10114	43083	2.69	0.00595	0.00535	-0.000119	0.000124	-0.0000409
	Medium (B)	16867	68723	2.70	0.0126	0.00211	-0.000219	0.0000634	0.00000196
	Fine (C)	70259	235196	2.68	0.0122	0.00856	-0.00000852	-0.0000756	-0.0000323

Table 2.2: Values of the three forces and three moments in/about x, y, z axes at 0 aoa for annular parachute

Canopy design	Mesh	Nodes	Elements	$F_z$ (N)	$F_y$ (N)	$F_x$ (N)	Mx	My	Mz
Annular	Coarse (D)	10351	40969	2.29	-0.000853	-0.0135	-0.0000114	0.000170	-0.0000101
	Medium (E)	39060	136032	2.34	0.0139	-0.00737	0.0000696	0.000199	-0.0000133
	Fine (F)	92768	297437	2.32	-0.00219	0.00229	-0.00000696	-0.0000518	0.0000268

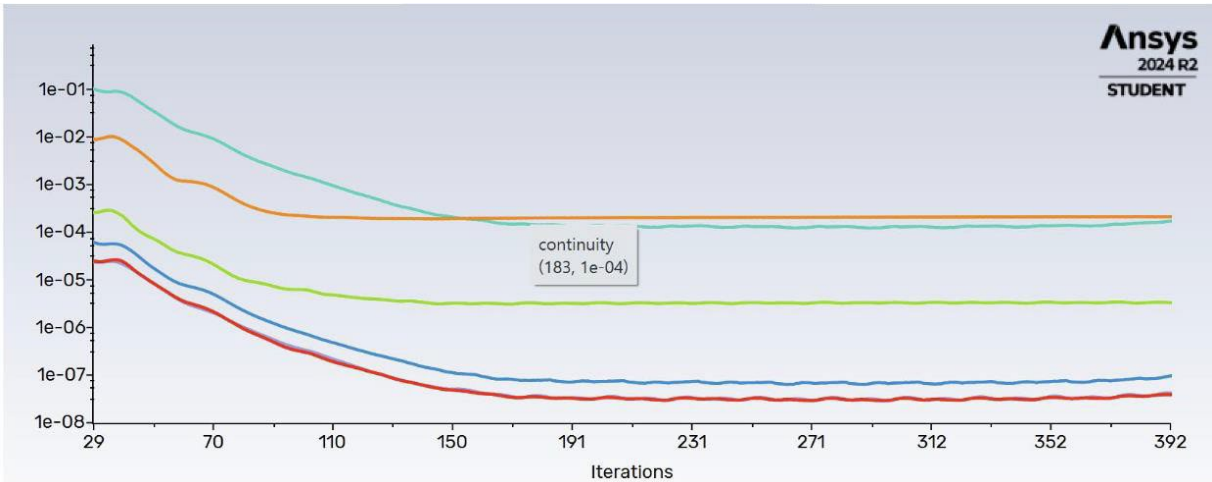


Fig. 3: Graph of residuals in CFD simulations

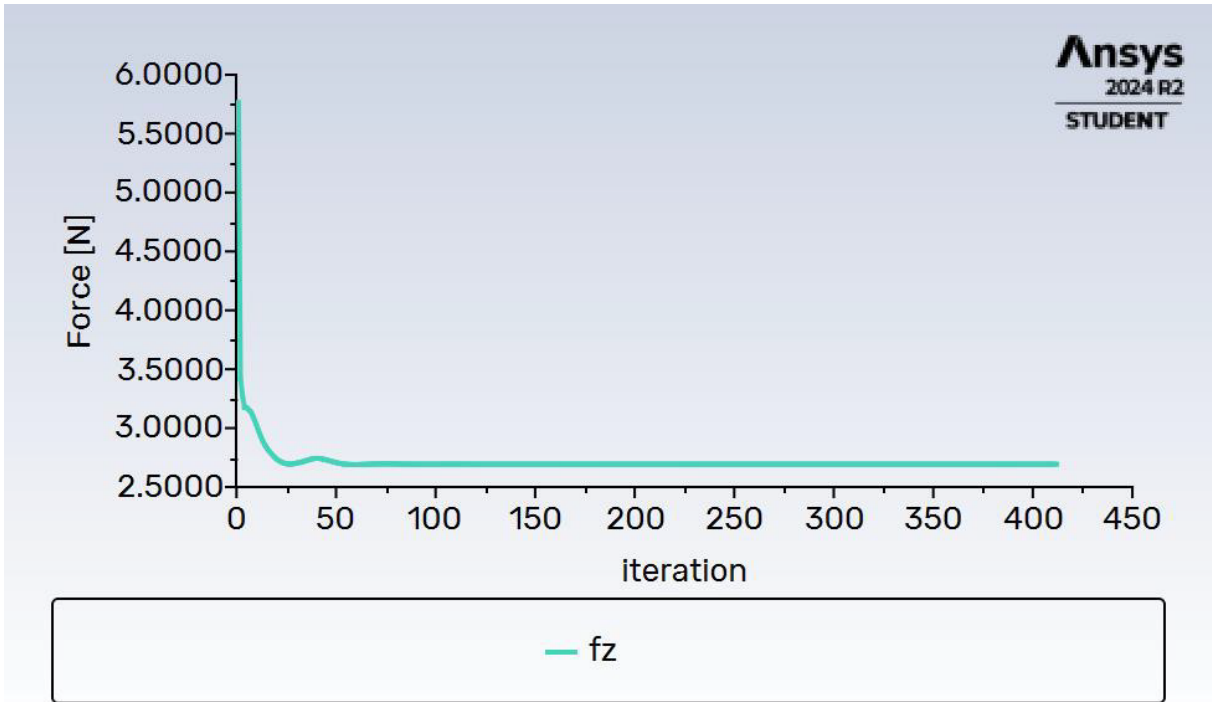


Fig. 4: Graph of force in z-axis in CFD simulation



(a)

(b)

Fig. 5: Parachute used in experimental drop test

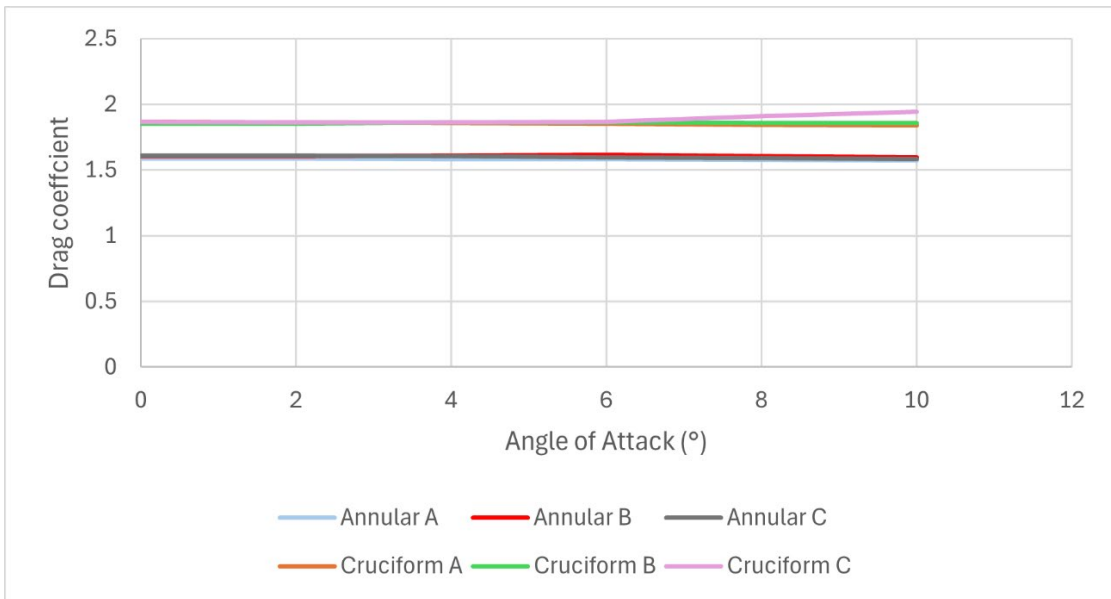


Fig. 6.1: Graph of drag coefficient against aoa from CFD

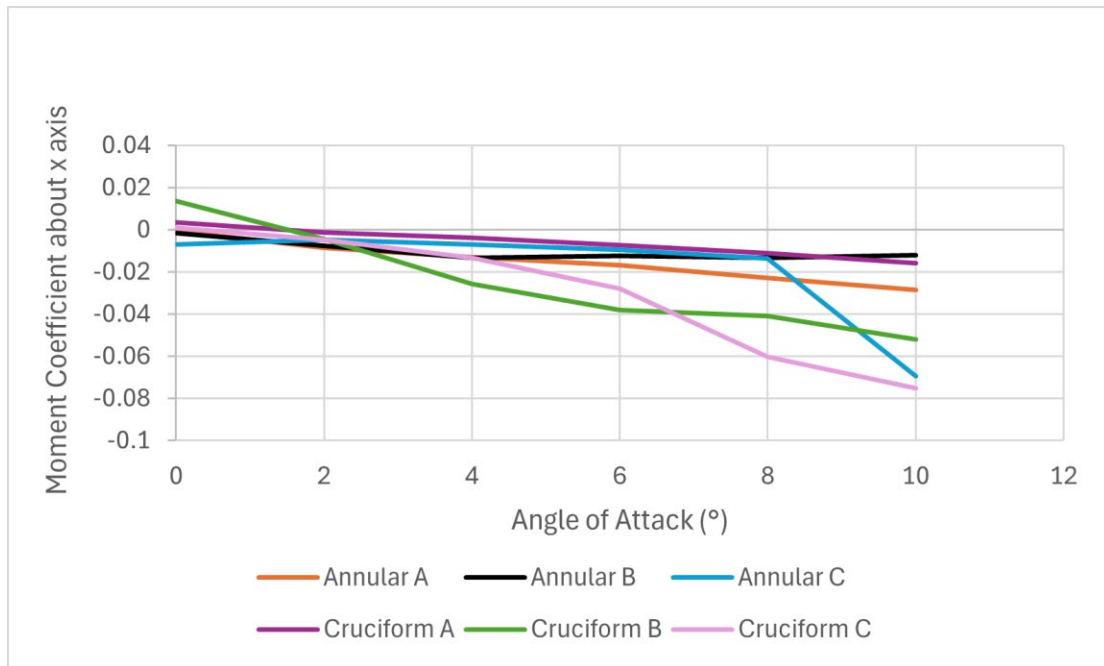


Fig. 6.2: Graph of moment coefficient about x-axis against aoa from CFD

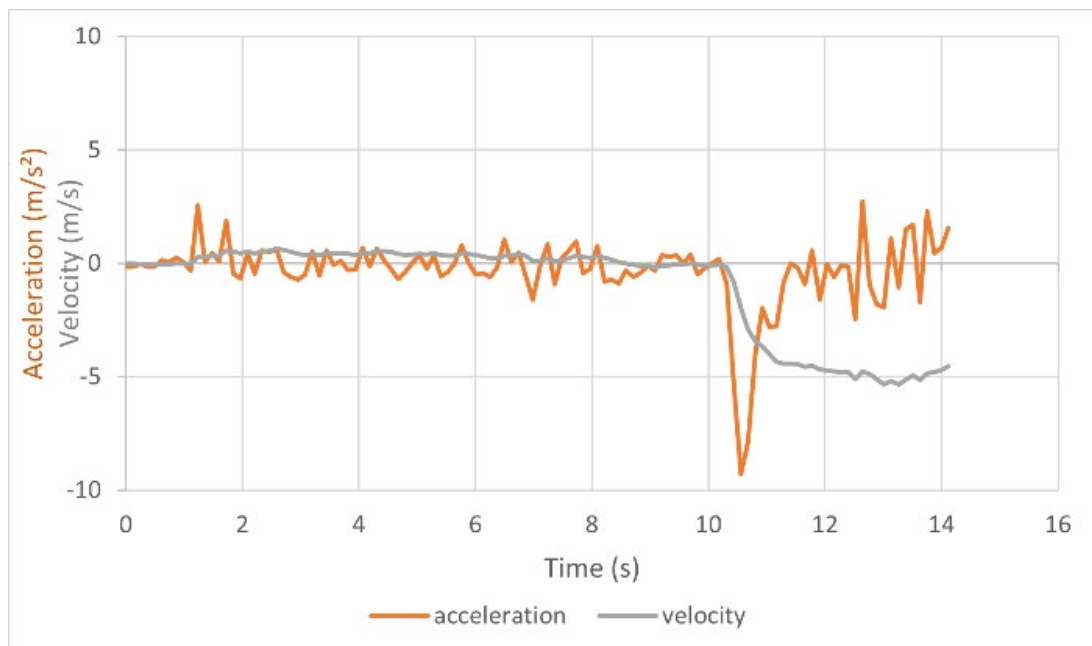


Fig. 6.3: Graph of acceleration and velocity in  $m/s^2$  and  $m/s$  respectively, against time in seconds from experimental data

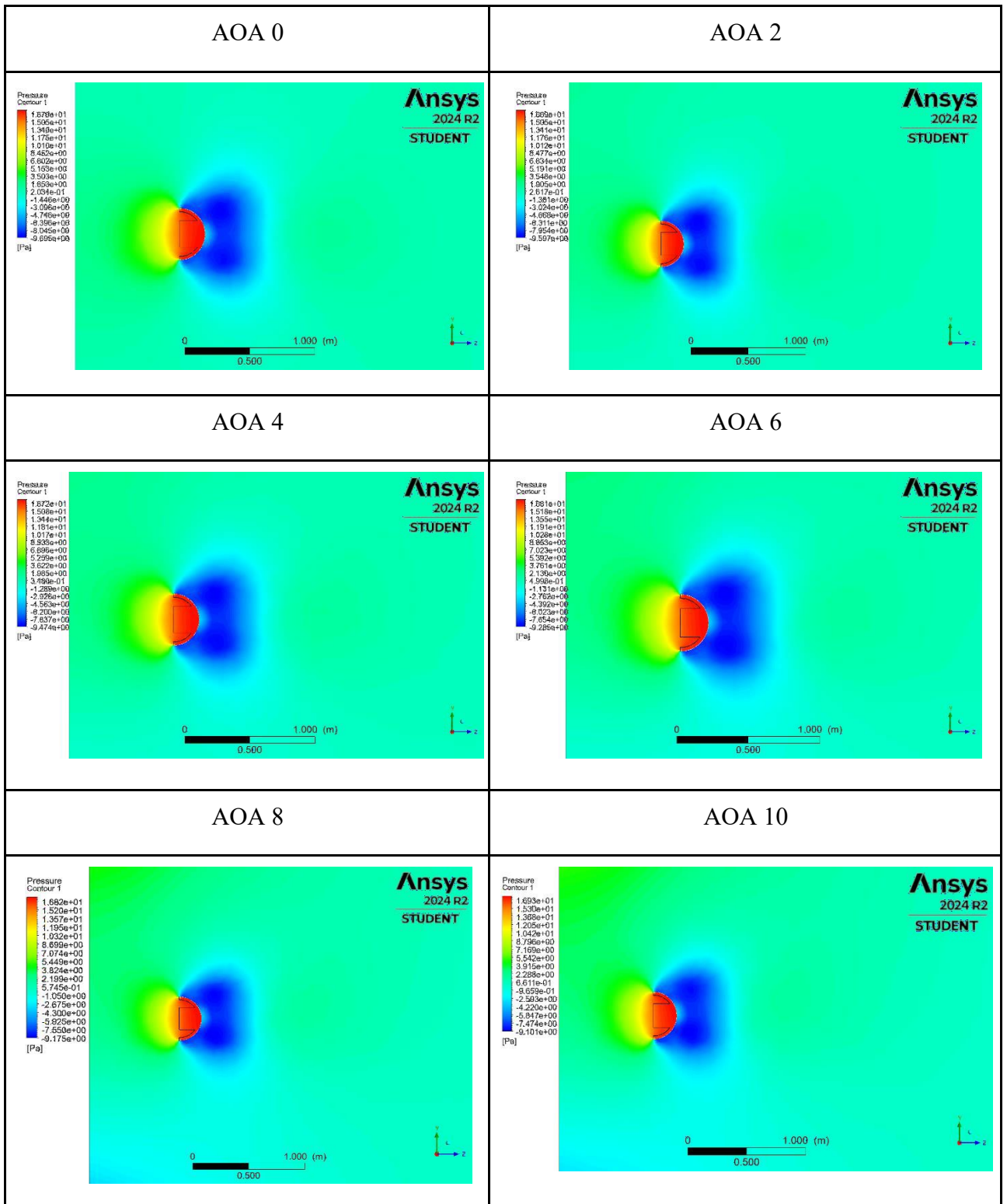


Fig. 7.1: Pressure contours on air at varying aoa for cruciform parachute

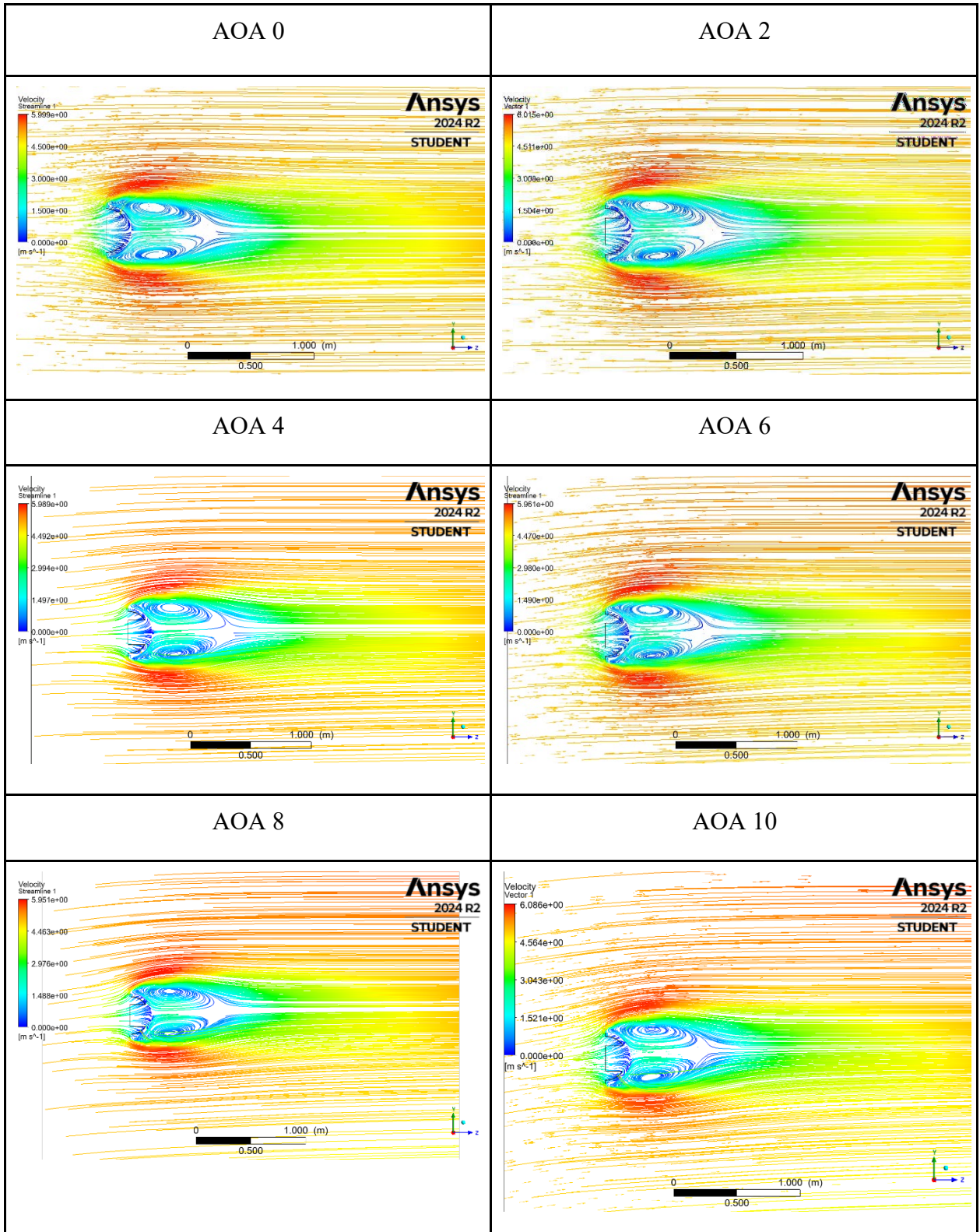


Fig. 7.2: Velocity streamlines at varying aoa for cruciform parachute

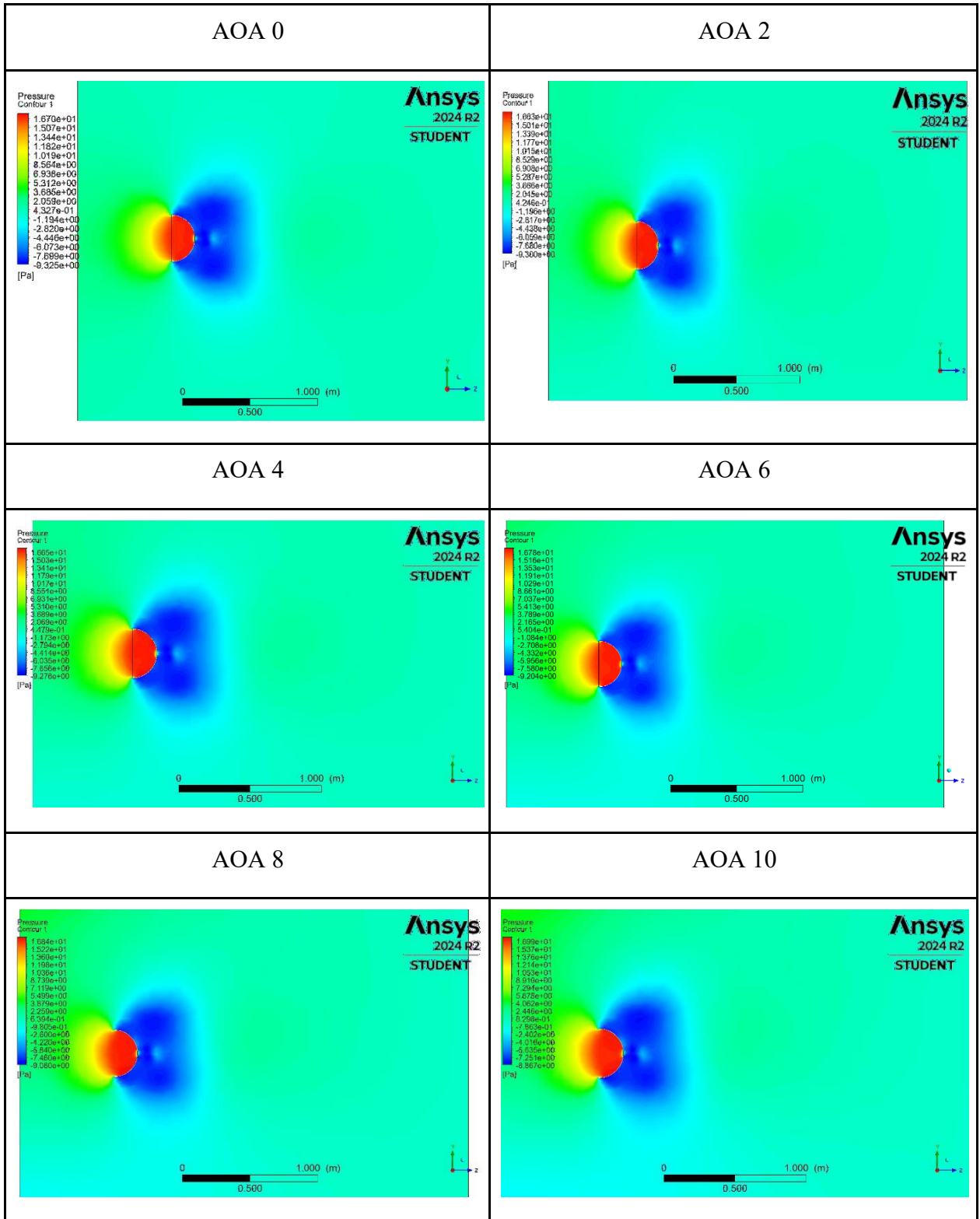


Fig. 8.1: Pressure contours on air at varying aoa for annular parachute

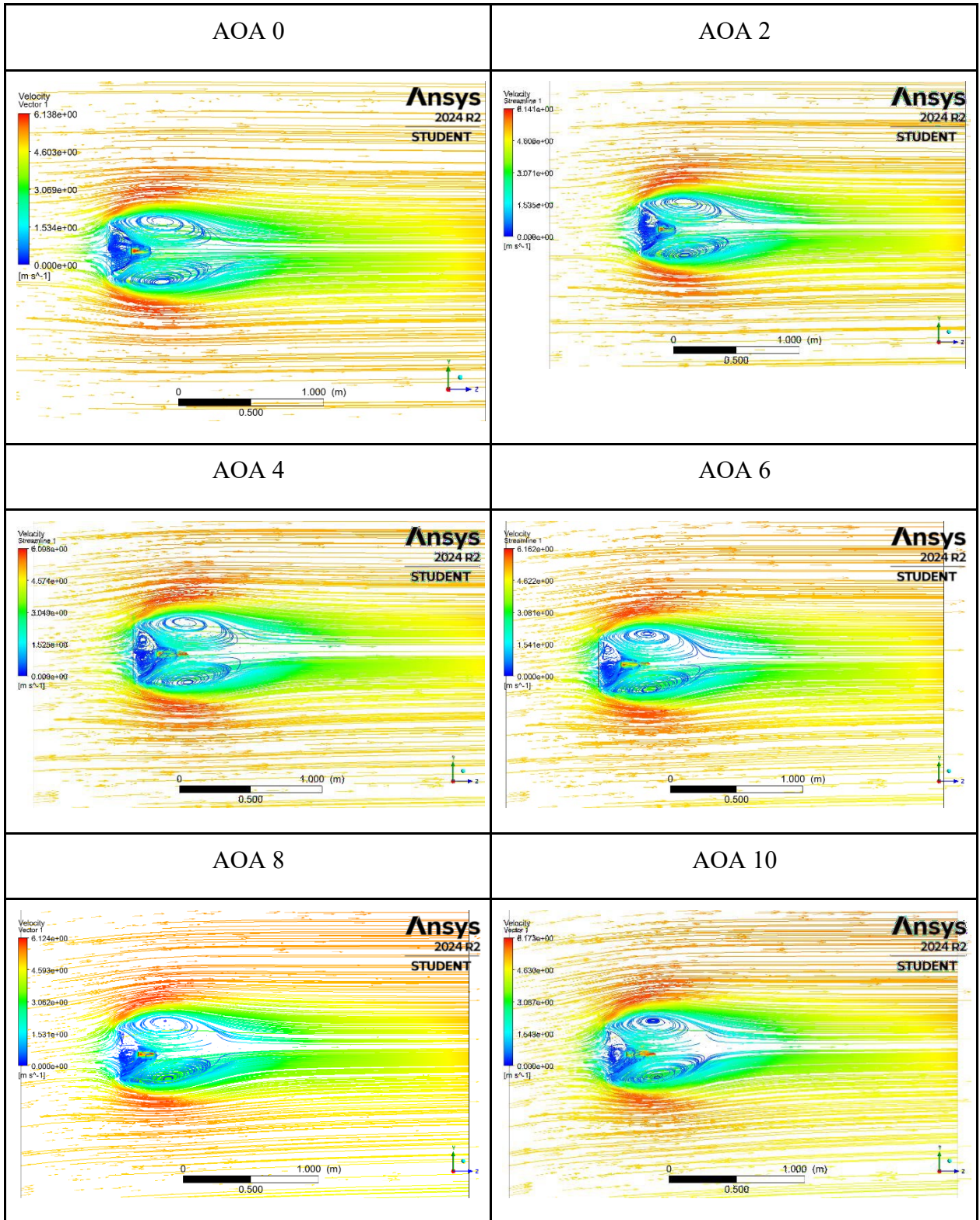


Fig. 8.2: Velocity streamlines at varying aoa for annular parachute